crystals

MDPI

*Article*

# A High-Performance Perovskite Solar Cell Prepared Based on Targeted Passivation Technology

**Meihong Liu [1], Yafeng Hao [1], Fupeng Ma [1], Pu Zhu [1], Huijia Wu [1], Ziwei Li [1], Wenyu Niu [1], Yujie Huang [1], Guitian Huangfu [2], Junye Li [2], Fengchao Li [1], Jiangang Yu [1], Tengteng Li [1,*], Longlong Zhang [3], Cheng Lei [1,*] and Ting Liang [1]**

[1] State Key Laboratory of Extreme Environment Optoelectronic Dynamic Measurement Technology and Instrument, North University of China, Taiyuan 030051, China
[2] Shanxi Zhonghaiwei Rail Transit Engineering Co., Ltd., Jinzhong 030699, China
[3] State Key Laboratory of Solar Activity and Space Weather, National Space Science Center, Chinese Academy of Sciences, Beijing 100730, China; zhanglonglong@nssc.ac.cn
* Correspondence: litengteng@nuc.edu.cn (T.L.); leicheng@nuc.edu.cn (C.L.)

**Abstract**

Perovskite materials have garnered significant attention in both fundamental research and practical applications owing to their exceptional light absorption coefficients, low fabrication costs, and inherent advantages for thin-film and flexible device fabrication. Nevertheless, interface defects within perovskite films induce detrimental non-radiative carrier recombination and pronounced hysteresis effects, which collectively impose substantial limitations on the photovoltaic performance and long-term operational stability of perovskite solar cells (PSCs). Conventional passivation strategies, despite their demonstrated efficacy in mitigating interface defects, often inadvertently introduce secondary defects in originally defect-free regions, thereby restricting the extent of device performance improvement. To overcome this critical limitation, we have developed a precision defect passivation methodology that employs a targeted two-step immersion–cleaning process, achieving selective defect passivation while concomitantly eliminating residual passivating agents. This approach effectively prevents the formation of new defects in unaffected regions of the perovskite films, and the resultant PSC possesses a power conversion efficiency (PCE) of 21.08%, accompanied by a substantial mitigation of hysteresis behavior. Furthermore, unencapsulated devices demonstrate remarkable stability, retaining over 81% of their initial efficiency after 20 days of atmospheric storage under 50% relative humidity, which underscores the effectiveness of our passivation strategy in simultaneously enhancing both device performance and operational stability.

**Keywords:** perovskite solar cells; targeted passivation technology; interface; stability

check for updates

Academic Editor: Leonid Kustov

Received: 15 August 2025
Revised: 11 September 2025
Accepted: 5 October 2025
Published: 8 October 2025

**Citation:** Liu, M.; Hao, Y.; Ma, F.; Zhu, P.; Wu, H.; Li, Z.; Niu, W.; Huang, Y.; Huangfu, G.; Li, J.; et al. A High-Performance Perovskite Solar Cell Prepared Based on Targeted Passivation Technology. *Crystals* **2025**, *15*, 873. https://doi.org/10.3390/cryst15100873

**Copyright:** © 2025 by the authors. Licensee MDPI, Basel, Switzerland. This article is an open access article distributed under the terms and conditions of the Creative Commons Attribution (CC BY) license (https://creativecommons.org/licenses/by/4.0/).

## 1. Introduction

The global transition toward sustainable energy systems has necessitated the development of efficient, cost-effective, and environmentally benign renewable energy solutions to address escalating energy crises and environmental degradation. As an inexhaustible and clean energy source, solar energy has emerged as a cornerstone of modern power generation technologies, playing an increasingly pivotal role in the global energy matrix. Among emerging photovoltaic technologies, perovskite solar cells (PSCs) have attracted significant attention since their inception due to their exceptional power conversion efficiency (PCE), low fabrication costs, straightforward manufacturing processes, and inherent compatibility

with thin-film and flexible device architectures, which collectively position them as leading candidates for next-generation photovoltaic applications. This paradigm-shifting potential was first demonstrated in 2009 when Miyasaka et al. introduced methylammonium perovskite materials as photosensitive layers in dye-sensitized solar cells [1], achieving an initial PCE of 3.8% and thereby initiating intensive research efforts in the PSC field that have subsequently driven remarkably rapid advancements, with certified power conversion efficiencies of single-junction PSCs now exceeding 27% [2]. Notwithstanding these remarkable achievements in efficiency enhancement, the large-scale commercialization of PSCs remains impeded by persistent challenges, particularly the critical bottleneck posed by interface defects, which substantially restrict both efficiency and long-term stability. These defects, which readily form at the interfaces between the perovskite layer, charge transport layers, and electrodes due to material lattice mismatches and chemical potential disparities, function as recombination centers that trap charge carriers, significantly compromising carrier separation and transport efficiencies while simultaneously accelerating interfacial chemical degradation, consequently leading to rapid performance deterioration under environmental stresses such as light irradiation and humidity exposure. Accordingly, effective passivation of interface defects through precise regulation of the interfacial chemical environment, targeted filling of defect sites, or strategic construction of protective layers has emerged as an essential approach for simultaneously suppressing non-radiative recombination and blocking degradation pathways, thereby representing a crucial technical lever for breaking through the performance limits of PSCs and facilitating their transition from laboratory-scale demonstrations to commercial applications [3–7].

Recent advances in interface passivation strategies have significantly advanced the performance and stability of PSCs [8–10]. Wu et al. developed a novel region-selective multisite organochlorine molecular passivation approach, distinct from conventional organic chloride passivation, and realized high-efficiency and stable PSCs. The researchers designed and synthesized two spatial isomers of tris(p-chlorophenyl)benzene (TCBP) containing three Cl atoms and found that when the distance between Cl atoms in the molecule is highly matched with the distance between iodide ions in perovskite, the unsaturated iodine vacancies can be better passivated. Compared with 1,3,5-tris(p-chlorophenyl)benzene, 1,2,4-tris(p-chlorophenyl)benzene has a stronger interaction with perovskite, which can provide a more efficient passivation effect. Using this organic molecule with the optimal Cl atom distribution, a PSC with a certified efficiency of 25.02% was achieved, and it could still maintain 90% of its initial efficiency after continuous operation for 500 h under continuous light irradiation [11]. Gu et al. proposed a multifunctional interface regulation strategy to improve the photovoltaic performance of PSCs by introducing dimethyl 2,2′-bipyridine-4,4′-dicarboxylate (DMCBPy) between the perovskite and PCBM layers. The 2,2′-bipyridine moiety in DMCBPy can strongly anchor the uncoordinated $Pb^{2+}$ ions on the perovskite surface through coordination, while the methyl ester groups in DMCBPy can adjust the surface polarity of the perovskite and improve the coverage of PCBM. In addition, the introduction of DMCBPy can regulate the interface energy level alignment and reduce non-radiative recombination. The prepared device achieved a maximum PCE of 25.04% and retained approximately 90% of its initial efficiency after aging for 1000 h in a nitrogen atmosphere at 85 °C [12]. Liu et al. proposed a passivation strategy analogous to two-dimensional perovskite interface passivation, which utilizes perovskite-like materials containing corner-, edge-, and face-sharing configurations simultaneously to construct an interface passivation layer. This stable and unique structure effectively inhibits the phenomenon of ion migration at the interface, enabling efficient carrier transport within the heterostructure. The perovskite solar cell based on such a “perovskite-like/perovskite heterojunction” achieved a certified quasi-steady-state photoelectric conversion efficiency

of 24.6% [13]. Xu et al. innovatively adopted the in situ polymerization interface bonding technology, which successfully enhanced the performance and stability of inverted PSCs. This technology forms multiple hydrogen bonds to anchor organic cations, inhibits the migration of halide ions, and generates a "molecular welding" effect. The champion device fabricated based on this strategy achieved a PCE of 26.25%, with an open-circuit voltage ($V_{oc}$) of 1.2 V and a fill factor (FF) increased to 85.2% [14]. The aforementioned works have provided various ideas for interface passivation of perovskite solar cells and achieved certain passivation effects. However, these passivation processes often involve directly spin coating or depositing passivation materials onto the interface to form a passivation covering layer. Introducing passivation materials in regions with high crystallinity and no interface defects is likely to be counterproductive, as it may introduce new defects. Therefore, a more reasonable passivation approach would be to introduce passivation materials specifically at defect sites while avoiding their introduction in other regions. Apparently, there is a lack of research reports in this aspect so far.

Herein, we have developed a precision-targeted interface defect passivation strategy through a synergistic computational–experimental approach. First-principles calculations were employed to systematically screen and identify 3-(aminomethyl)pyridinium (3AMPY) as the optimal passivation agent, demonstrating superior defect passivation potential. The targeted passivation process was achieved through a two-step protocol involving controlled immersion of perovskite films in a 3AMPY solution to facilitate specific defect-passivating interactions, followed by ethyl acetate rinsing to selectively eliminate unreacted 3AMPY molecules and potential reaction byproducts. This approach effectively passivates interface defects while preventing the formation of residual passivation layers. The resultant PSC exhibits a PCE of 21.08%, accompanied by significant mitigation of hysteresis behavior. Moreover, the unencapsulated device can still retain over 81% of its initial efficiency after being stored in an atmospheric environment (50% relative humidity) for 20 days, demonstrating exceptional operational stability and underscoring the effectiveness of our passivation strategy in enhancing both device performance and long-term reliability.

## 2. Experiment

### 2.1. Materials

3-(aminomethyl)pyridinium (3AMPY), lead iodide ($PbI_2$), methylammonium iodide (MAI), formamidinium iodide (FAI), methylammonium chloride (MACl), poly(triarylamine) (PTAA), and phenyl-C61-butyric acid methyl ester ($PC_{61}BM$) were purchased from Xi'an Yuri Solar Co., Ltd. (Xi'an, China) Solvents such as chloroform, ethyl acetate, chlorobenzene, N,N-dimethylformamide (DMF), and dimethylsulfoxide (DMSO) were purchased from Sigma-Aldrich (St. Louis, MO, USA). Indium tin oxide (ITO) conductive glasses were purchased from Yingkou Youxuan Tech Co., Ltd. (Yingkou, China).

### 2.2. Device Fabrication

Prior to the experiment, the ITO substrates were subjected to a rigorous cleaning protocol that involved sequential ultrasonication in toluene, acetone, isopropanol, and deionized water for 10 min per solvent, followed by nitrogen blow drying and 30 min of ultraviolet–ozone treatment to ensure optimal surface hydrophilicity and the removal of organic contaminants. The $PbI_2$ solution was prepared by dissolving 1.3 mmol of $PbI_2$ in a mixed solvent consisting of 0.95 mL of DMF and 0.05 mL of DMSO. The FAI solution was prepared by dissolving 60 mg of FAI, 6 mg of MAI, and 6 mg of MACl in 1 mL of isopropanol. The device fabrication commenced with the deposition of a hole transport layer (HTL) by spin coating a 10 mg/mL PTAA solution in toluene onto the cleaned ITO substrates at 5000 rpm for 30 s, followed by thermal annealing at 100 °C for 10 min. After

the substrate was cooled to room temperature, a $PbI_2$ film was spin-coated onto the PTAA layer at 2000 rpm, followed by annealing at 70 °C for 1 min. Immediately afterward, a layer of FAI solution was spin-coated onto the $PbI_2$ film at 2000 rpm, followed by annealing at 150 °C for 15 min to form the perovskite film. Then, the perovskite film was statically treated with a 3AMPY solution (diluted 50-fold with chloroform) for 10 s, followed by solvent removal via spin coating and cleaning with ethyl acetate for 10 s. After cleaning for 10 s, the solvent was spun off, and the film was annealed at 100 °C for 3 min to thoroughly remove residual solvents. Once the film cooled to room temperature again, a $PC_{61}BM$ electron transport layer (10 mg/mL in chlorobenzene) was spin-coated onto its surface at 3000 rpm, and a 100 nm thick silver electrode was thermally evaporated under vacuum to complete the device.

### *2.3. Characterization*

The current density–voltage (J-V) characteristics and maximum power point (MPP) tracking were performed under standard AM 1.5 G illumination (100 $mW/cm^2$) using an ABET SUN 3000 solar simulator coupled with a Keithley 2400 source measurement unit, with light intensity calibrated using a reference silicon photodiode (ABET Technology, Milford, CT, USA). External quantum efficiency (EQE) measurements were conducted with a Newport QE-PV-SI system incorporating a high-resolution monochromator and precision source meter. Crystallographic analysis was performed using a Rigaku SmartLab 3000 X-ray diffractometer (XRD, Rigaku, Tokyo, Japan). Microstructural characterization was performed using a JEOL JSM-6340 scanning electron microscope (SEM, JEOL, Tokyo, Japan).

## 3. Results and Discussion

Prior to the initiation of the passivation process, we first analyzed the formation energies between several common passivation materials and perovskite through first-principles calculations, as shown in Figure 1. The calculation results indicate that the formation energies of 3-(aminomethyl)pyridinium (3AMPY), phenethylammonium iodide (PEAI), and 4-aminomethylpyridinium (4AP) with perovskite are −7.44 eV, −6.96 eV, and −6.90 eV, respectively, demonstrating that 3AMPY exhibits the strongest interaction with perovskite due to its significantly lower formation energy, thereby indicating a superior defect passivation capability [15–19]. Based on the theoretical calculation results, 3AMPY was selected as the optimal interface passivation material. The targeted passivation process was implemented through a controlled two-step protocol involving “soaking” and “cleaning,” as depicted in Figure 2a. After the perovskite film was prepared using the traditional two-step method, we dropped a certain amount of 3AMPY solution (diluted with chloroform) onto the surface of the perovskite film and maintained in static contact for approximately 10 s (soaking stage). Upon completion of soaking, the solution on the film surface was spin-dried at 5000 rpm to achieve uniform drying. Subsequently, ethyl acetate solvent was further dropped onto the surface to dissolve the residual substances, which were then quickly removed by spin-drying (cleaning stage). As shown in Figure 2b, the as-prepared perovskite film (prior to soaking) exhibited numerous intrinsic defects and contained residual unreacted $PbI_2$. The soaking process facilitated targeted passivation of these defects by 3AMPY, with residual $PbI_2$ potentially reacting with 3AMPY to form a two-dimensional perovskite structure. However, unreacted 3AMPY or other derived intermediates tended to accumulate at the grain boundaries (Figure 2c). The subsequent cleaning stage effectively removed these residual species, preventing the introduction of new defects into the perovskite film (Figure 2d), ultimately resulting in a high-quality perovskite film with significantly reduced defect density.

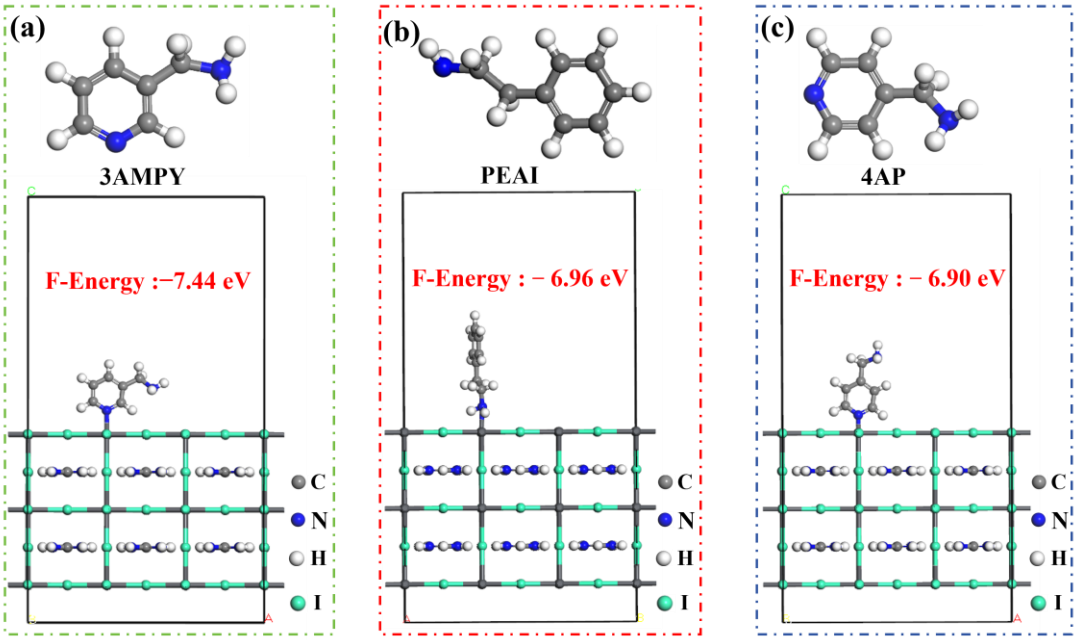



**Figure 1.** First-principles formation energy calculations of (**a**) 3AMPY, (**b**) PEAI, and (**c**) 4AP.

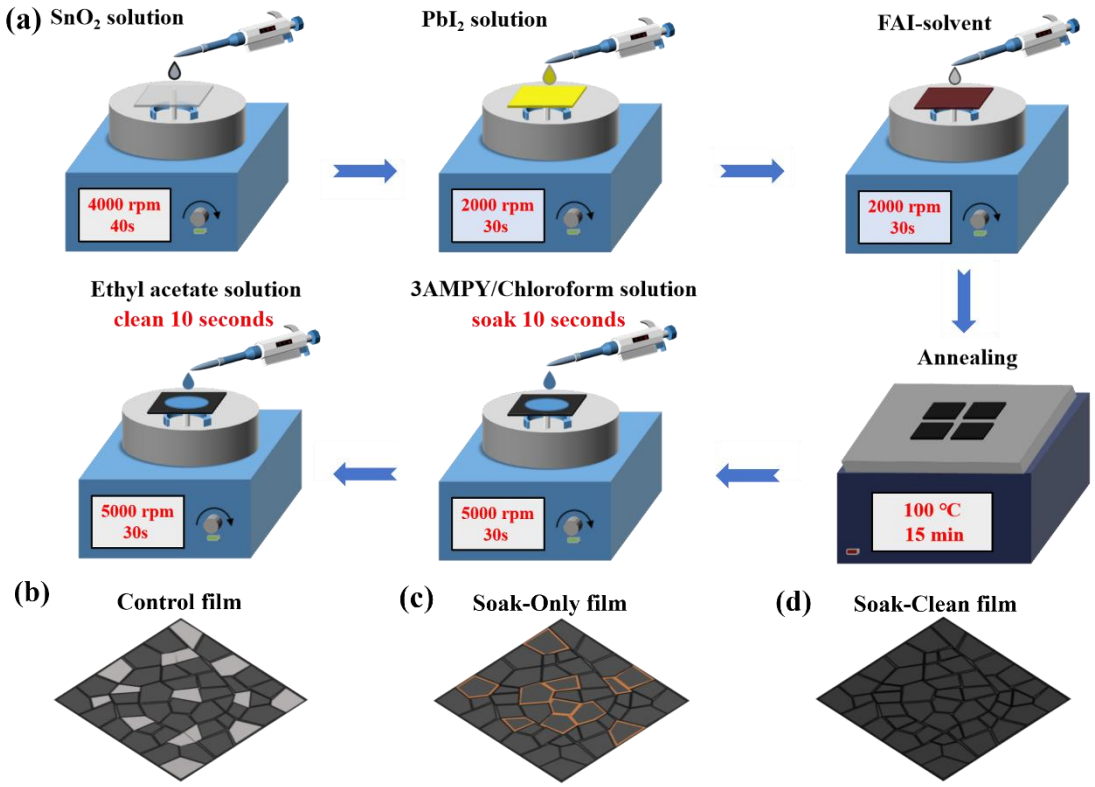



**Figure 2.** (**a**) Schematic diagram of the immersion–cleaning process flow; (**b**) schematic diagram of the control perovskite film; (**c**) schematic diagram of the perovskite film after soaking; (**d**) schematic diagram of the perovskite film after soaking–cleaning.

To verify the advantages of the soak–clean passivation process, we systematically compared the photovoltaic performance of solar cells fabricated using control (untreated), soak-only (3AMPY-treated without cleaning), and soak–clean (3AMPY-treated followed by cleaning) perovskite films, with the device structure configured as ITO/PTAA/perovskite-3AMPY/$PC_{61}BM$/Ag, as shown in Figure 3a. From the cross-sectional SEM images, it can be seen that the thickness of the perovskite active layer is approximately 600 nm, the

thickness of $PC_{61}BM$ is 70 nm, and the thickness of ITO is about 130 nm (Figure S1). The 3AMPY passivation layer is difficult to observe via SEM due to its low thickness. The comprehensive performance metrics of different devices are summarized in Table 1. The control device exhibited an average PCE of 18.47% with a maximum efficiency of 19.29% (see the J-V curve in Figure 3b), while the soak-only process improved the average PCE to 19.99%, demonstrating that 3AMPY effectively passivates perovskite film defects and enhances device performance. Notably, the subsequent clean process further elevated the average PCE to 20.48%, with a peak efficiency reaching 21.08%, confirming that the clean step significantly reduces residual defects in the perovskite film. To validate the accuracy of the J-V test performance, we further measured the external quantum efficiency (EQE) of different solar cells (Figure 3c). The short-circuit current densities ($J_{sc}$) integrated from the EQE spectra (22.23 $mA/cm^2$ for control, 22.30 $mA/cm^2$ for soak-only, and 22.44 $mA/cm^2$ for soak–clean devices) exhibited less than 5% deviation from the corresponding J-V values, thereby verifying the reliability of our J-V performance characterization. Furthermore, although the soak-only device showed improved performance compared to the control, it exhibited aggravated hysteresis behavior with a hysteresis factor of 5.9%, whereas the clean process effectively eliminated hysteresis (hysteresis factor reduced to 1.3%) as evidenced by the J-V curves (Figure 3d–f and Table S1–S3). This phenomenon can be attributed to the following mechanisms: during the soak process, although 3AMPY repairs perovskite film defects, excess 3AMPY molecules and reaction intermediates accumulate at perovskite grain boundaries, which not only impede interfacial carrier transport but also induce secondary defects, thereby exacerbating hysteresis; conversely, the clean process removes these detrimental residues via ethyl acetate treatment, preventing new defect formation and consequently eliminating hysteresis. To further substantiate this conclusion, we conducted comprehensive morphological and structural characterizations on perovskite films under different processing conditions.

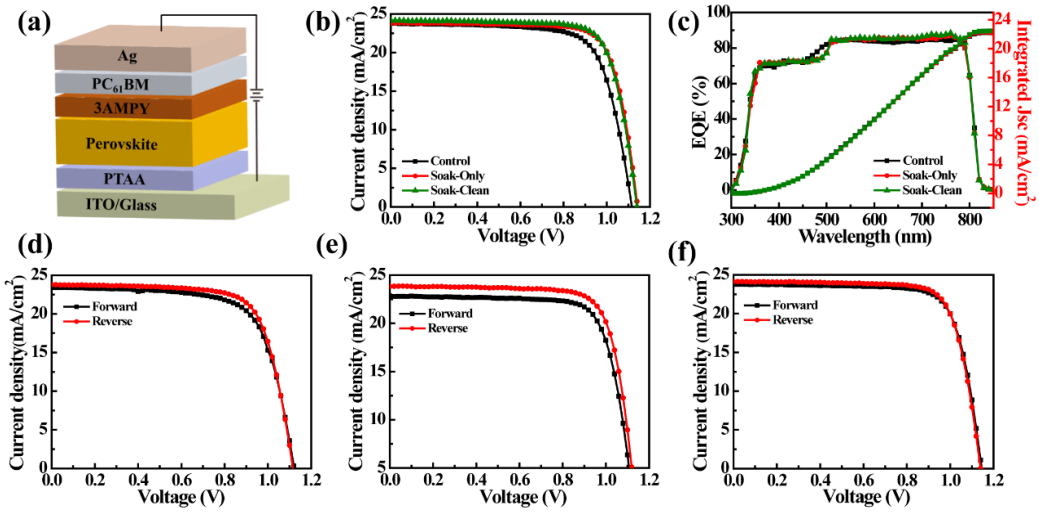



**Figure 3.** (**a**) Schematic diagram of the device structure; (**b**) J-V characteristic curves of different devices; (**c**) EQE test curves; (**d**) forward and reverse scan J-V characteristic curves of the control device; (**e**) forward and reverse scan J-V characteristic curves of the soak-only device; (**f**) forward and reverse scan J-V characteristic curves of the soak–clean device.

Figure 4a–c present the scanning electron microscopy (SEM) images of the surfaces of different perovskite films, revealing notable differences in their microstructural characteristics. It can be seen from the SEM images that the grain size of the three different perovskite films is approximately 300–1000 nm. The control perovskite film surface is prominently covered with numerous residual $PbI_2$ particles and surface hole defects, such defects that

typically act as carrier traps during charge transport, facilitating non-radiative recombination and inducing energy loss, which collectively contribute to the degradation of device performance. In contrast, following the soak process, the residual $PbI_2$ particles and hole defects are nearly eliminated, demonstrating that 3AMPY effectively repairs the surface defects of the perovskite film and reacts with $PbI_2$ to form a two-dimensional perovskite phase, thereby further passivating interface defects. Nevertheless, a certain amount of residue remains observable at the grain boundaries of the film, which is likely to generate new defects, impede carrier mobility, and exacerbate the hysteresis phenomenon. After the subsequent clean process, the residues at the crystalline regions are almost completely removed, resulting in a perovskite film with a flat, dense, and smooth morphology that represents an ideal active layer structure for perovskite devices. X-ray diffraction (XRD) measurements yielded consistent results, as shown in Figure 4d–f. The control perovskite film exhibits a strong $PbI_2$ peak at 12.5°, indicative of incomplete conversion of $PbI_2$ during the conventional two-step synthesis process and the presence of substantial defects. Upon completion of the soak process, the $PbI_2$ peak intensity diminishes significantly, while the characteristic perovskite peak (at 14°) intensifies markedly, suggesting that 3AMPY not only reduces film defects but also enhances the overall crystallinity of the perovskite. However, a distinct minor peak emerging at 12° is attributed to an intermediate product formed by the reaction of residual 3AMPY with $PbI_2$, which is completely absent after the clean process, confirming the effective removal of these residues. Collectively, the combined SEM and XRD results demonstrate that the sequential soak–clean processes achieve the dual benefits of effective perovskite film defect passivation, improved crystallinity, and complete elimination of residues generated during the passivation process, ultimately yielding a perovskite film with high crystallinity, low defect density, and an absence of residual substances.

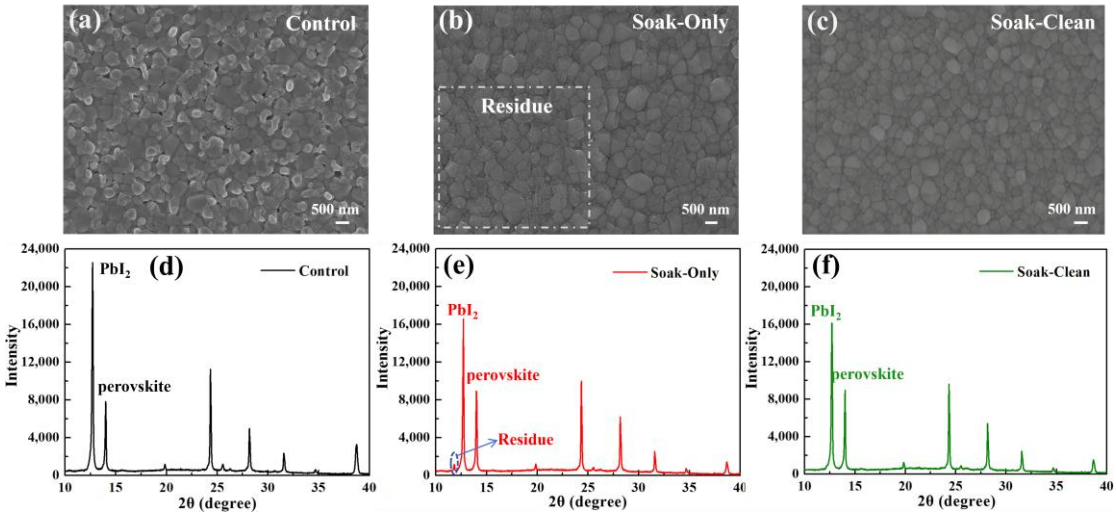



**Figure 4.** (**a**) SEM images of the control perovskite film; (**b**) SEM images of the soak-only perovskite film; (**c**) SEM images of the soak–clean perovskite film; (**d**) XRD test results of the control perovskite film; (**e**) XRD test results of the soak-only perovskite film; (**f**) XRD test results of the soak–clean perovskite film.

To further investigate the carrier transport behavior in perovskite films fabricated through different processing methods, we systematically measured the steady-state photoluminescence (PL) spectra of both Glass/Perovskite and ITO/PTAA/Perovskite/$PC_{61}BM$ structures as depicted in Figure 5a,b. The PL intensity analysis reveals that in the absence of carrier transport layers, the perovskite film prepared via the soak–clean process exhibits the highest PL intensity, indicative of minimal non-radiative recombination losses arising from

defect states, followed by the soak-only and control films, respectively. Conversely, when carrier transport layers are incorporated, the soak–clean perovskite film demonstrates the lowest PL intensity, suggesting highly efficient and rapid carrier extraction and transport. These PL results conclusively demonstrate that the soak–clean process produces perovskite films with the lowest defect density and the highest carrier transfer efficiency, thereby contributing to optimal device performance characterized by minimal hysteresis [20–22]. Complementary transient photocurrent (TPC) and transient photovoltage (TPV) measurements of different perovskite devices, presented in Figure 5c,d, further elucidate the carrier dynamics. The TPC decay characteristics reveal that the soak–clean device exhibits a slightly shorter carrier transit time compared to both control and soak-only devices, indicating a marginally enhanced carrier transport rate. More significantly, the TPV results demonstrate a substantial difference in charge carrier recombination dynamics, with the soak–clean device showing a markedly longer TPV decay time relative to the control and soak-only devices. Given that TPV decay time correlates inversely with defect density (where longer decay times correspond to fewer trap states), this observation provides definitive evidence for the reduced defect concentration in the soak–clean device [23,24]. The comprehensive PL, TPV, and TPC characterization results exhibit remarkable consistency with the previously discussed SEM and XRD findings, collectively confirming that the soak–clean process represents a superior passivation strategy as it simultaneously achieves effective defect repair while preventing the introduction of additional defects through residual passivation materials.

**Table 1.** Photovoltaic performance of different PSCs. The data were obtained based on 30 cells for each condition.

| Sample | $V_{oc}$ (V) | $J_{sc}$ (mA/cm$^2$) | FF(%) | Average PCE (%) | Best PCE (%) |
|---|---|---|---|---|---|
| Control | 1.101 ± 0.010 | 23.22 ± 0.35 | 72.24 ± 0.48 | 18.47 ± 0.38 | 19.29 |
| Soak-Only | 1.134 ± 0.006 | 23.33 ± 0.42 | 75.50 ± 0.60 | 19.99 ± 0.52 | 20.90 |
| Soak–Clean | 1.140 ± 0.006 | 23.68 ± 0.21 | 75.87 ± 0.47 | 20.48 ± 0.29 | 21.08 |

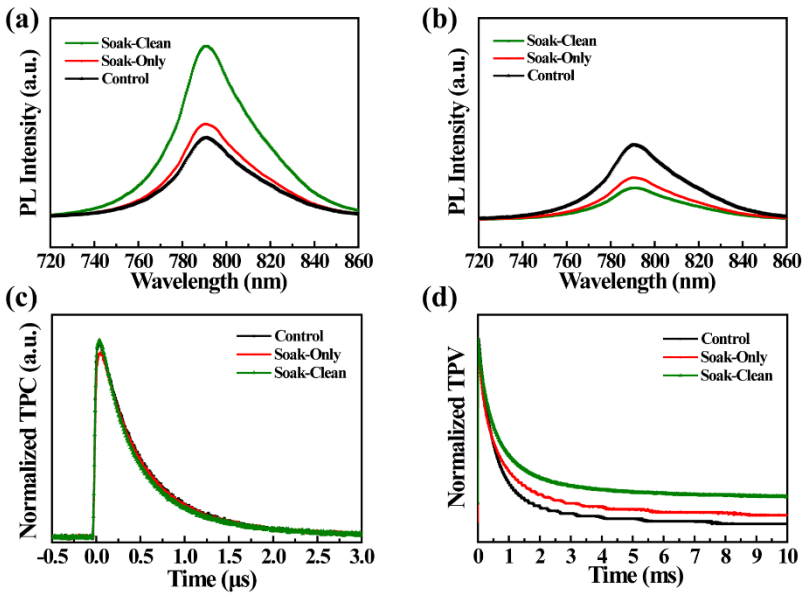



**Figure 5.** (**a**) PL test of perovskite films without transport layer; (**b**) PL test of perovskite films with transport layer; (**c**) transient photocurrent test; (**d**) transient photovoltage test.

Finally, we conducted a comprehensive comparative analysis of the stability of different perovskite devices, as illustrated in Figure 6a, which presents the environmental

stability test results (maintained at approximately 50% relative humidity) for control, soak-only, and soak–clean devices. After 20 days of atmospheric storage, the control device exhibited a significant performance degradation, retaining only 52% of its original efficiency, the soak-only device demonstrated superior stability with 73% efficiency retention, and the soak–clean device achieved the most remarkable performance preservation, maintaining 81% of its initial efficiency. This enhanced stability can be attributed to the following two key factors: Firstly, the perovskite film with substantially reduced defect density, improved surface flatness, and enhanced crystalline packing exhibits superior resistance to moisture-induced degradation. Secondly, the partial formation of two-dimensional perovskite phases through the reaction between residual 3AMPY and $PbI_2$ significantly increases the hydrophobicity of the film surface, thereby providing additional protection against environmental moisture ingress. Figure 6b presents the maximum power point (MPP) tracking results under continuous operational conditions, which corroborate the environmental stability findings, demonstrating that the soak–clean device exhibits optimal long-term operational stability with negligible performance degradation during 400 s of continuous maximum power output, in stark contrast to the control and soak-only devices which both exhibited measurable efficiency losses under identical testing conditions.

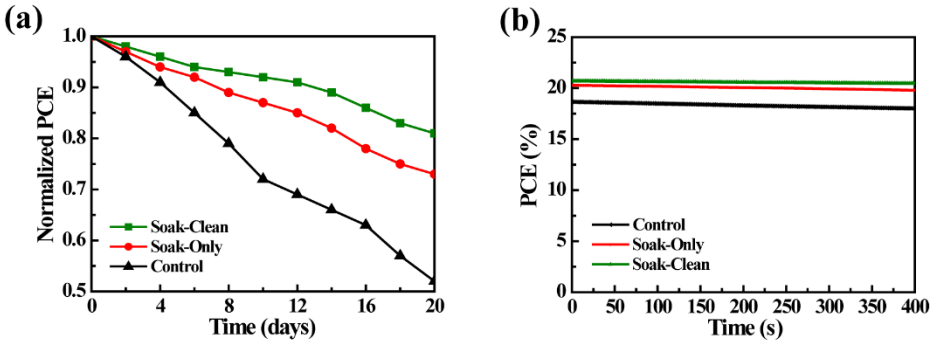



**Figure 6.** (**a**) Humidity stability tests of different devices; (**b**) maximum power point tests of different devices.

## 4. Conclusions

In this work, we developed a novel "soak–clean" targeted passivation strategy to overcome the limitations of conventional interface passivation methods in PSCs, which frequently introduce secondary defects through residual passivation material deposition. Leveraging first-principles calculations, we identified 3AMPY as an optimal passivation agent and achieved its targeted interaction with perovskite defects through a precisely controlled two-step process involving sequential immersion of the perovskite film in a chloroform-diluted 3AMPY solution followed by ethyl acetate cleaning. Comprehensive structural and morphological characterizations confirmed that the soak step effectively repairs intrinsic film defects, including residual lead iodide and surface voids, through the formation of stable two-dimensional perovskite phases with 3AMPY, while the subsequent clean step selectively removes unreacted 3AMPY molecules and intermediate reactions, thereby eliminating potential defect sources at grain boundaries. This synergistic dual-step approach yields a perovskite film exhibiting high crystallinity, low defect density, and an ideal flat, dense morphology. Device performance evaluations revealed that inverted PSCs treated with this soak–clean process achieved a champion PCE of 21.08% accompanied by significant hysteresis reduction. This "soak–clean" approach provides a facile and effective route to achieve targeted defect passivation without introducing residual-induced defects, offering valuable insights for the development of high-performance and stable PSCs.

**Supplementary Materials:** The following supporting information can be downloaded at: https://www.mdpi.com/article/10.3390/cryst15100873/s1, Figure S1: cross-sectional SEM images of the perovskite film; Table S1: hysteresis dates of control device; Table S2: Hysteresis dates of soak-only device; Table S3: Hysteresis dates of soak-clean device.

**Author Contributions:** Conceptualization, Y.H. (Yafeng Hao); Methodology, M.L., F.M. and P.Z.; Software, G.H. and J.L.; Formal analysis, H.W. and Z.L.; Investigation, W.N. and Y.H. (Yujie Huang); Data curation, M.L. and C.L.; Writing—original draft, M.L.; Writing—review & editing, M.L.; Visualization, F.L. and J.Y.; Project administration, T.L. (Tengteng Li), L.Z. and T.L. (Ting Liang); Funding acquisition, T.L. (Tengteng Li) and L.Z. All authors have read and agreed to the published version of the manuscript.

**Funding:** This work was supported by the National Natural Science Foundation of China (Nos. 62405293, 62301509 and 62304209), the Key Research and Development Program of Shanxi Province (No. 202302030201001) and the Fundamental Research Program of Shanxi Province (No. 202303021212191, 202203021222079, 20210302123203 and 202103021223185).

**Data Availability Statement:** The original contributions presented in this study are included in the article/Supplementary Material. Further inquiries can be directed to the corresponding authors.

**Conflicts of Interest:** Author Guitian Huangfu and Junye Li were employed by the company Shanxi Zhonghaiwei Rail Transit Engineering Co., Ltd. The remaining authors declare that the research was conducted in the absence of any commercial or financial relationships that could be construed as a potential conflict of interest.

## References

1. Kojima, A.; Teshima, K.; Shirai, Y.; Miyasaka, T. Organometal Halide Perovskites as Visible-Light Sensitizers for Photovoltaic Cells. *J. Am. Chem. Soc.* **2009**, *131*, 6050–6051. [CrossRef]
2. Best Research-Cell Efficiency Chart. Available online: https://www.nrel.gov/pv/cell-efficiency.html (accessed on 1 December 2023).
3. Cao, Y.; Gao, F.; Xiang, L.; Li, H.; Li, D.; Liu, Q.; Liu, H.; Zou, C.; Li, S. Defects Passivation Strategy for Efficient and Stable Perovskite Solar Cells. *Adv. Mater. Interfaces* **2022**, *9*, 2200179. [CrossRef]
4. Das, C.; Roy, R.; Kedia, M.; Kot, M.; Zuo, W.; Félix, R.; Sobol, T.; Flege, J.I.; Saliba, M. Unraveling the Role of Perovskite in Buried Interface Passivation. *ACS Appl. Mater. Interfaces* **2023**, *15*, 56500–56510. [CrossRef] [PubMed]
5. Kim, S.J.; Kim, Y.; Chitumalla, R.K.; Ham, G.; Nguyen, T.-D.; Jang, J.; Cha, H.; Milić, J.; Yum, J.-H.; Sivula, K.; et al. Interfacial engineering through lead binding using crown ethers in perovskite solar cells. *J. Energy Chem.* **2024**, *92*, 263–270. [CrossRef]
6. Liu, J.; He, Y.; Ding, L.; Zhang, H.; Li, Q.; Jia, L.; Yu, J.; Lau, T.W.; Li, M.; Qin, Y.; et al. Perovskite/silicon tandem solar cells with bilayer interface passivation. *Nature* **2024**, *635*, 596–603. [CrossRef] [PubMed]
7. Huang, L.; Lou, Y.H.; Wang, Z.K. Buried Interface Passivation: A Key Strategy to Breakthrough the Efficiency of Perovskite Photovoltaics. *Small* **2023**, *19*, 2302585. [CrossRef]
8. Liang, A.; Feng, C.; Yang, Y.; Liu, J.; Yang, J.; Xie, G.; Huang, F.; Chen, Y. Biomimetic Mineralization Nucleation with Polymer Template Enabled High-Performance Perovskite Solar Cells by Anti-Solvent-Free Technology. *Adv. Mater.* **2025**, *37*, 2507401. [CrossRef]
9. Akman, E.; Pirzado, A.A.A.; Aftab, S.; Ebic, M.; Al-Kahtani, A.A.; Mohammed, M.K.A.; Gulen, M.; Aftabuzzaman, M.; Uzun, O.; Jie, J. Benefitting from methylene blue dye molecule for improving performance of perovskite photovoltaics. *J. Power Sources* **2025**, *665*, 238010. [CrossRef]
10. Chen, W.; Shai, X.; Liu, X.; Yu, Y.; He, D.; Zeng, C.; Song, Y.; Chen, J. Simultaneous targeted therapy of multiple top interface defects for high-performance air-processed n-i-p perovskite solar cells. *Chem. Eng. J.* **2025**, *520*, 166301. [CrossRef]
11. Wu, J.; Li, M.H.; Fan, J.T.; Li, Z.; Fan, X.-H.; Xue, D.-J.; Hu, J.-S. Regioselective Multisite Atomic-Chlorine Passivation Enables Efficient and Stable Perovskite Solar Cells. *J. Am. Chem. Soc.* **2023**, *145*, 5872–5879. [CrossRef]
12. Gu, W.M.; Zhao, M.; Wang, Q.; Gong, K.; Li, X.; Sun, Y.; Sun, S.; Yang, G.; Hu, C.; Jiang, K.-J. Regulating perovskite/PCBM interfacefor highly efficient and stable inverted perovskite solar cells. *Chem. Eng. J.* **2025**, *509*, 161237. [CrossRef]
13. Liu, C.; Yang, Y.; Chen, H.; Spanopoulos, I.; Bati, A.S.R.; Gilley, I.W.; Chen, J.; Maxwell, A.; Vishal, B.; Reynolds, R.P.; et al. Two-Dimensional Perovskitoids Enhance Stabilityin Perovskite Solar Cells. *Nature* **2024**, *633*, 359–364. [CrossRef] [PubMed]
14. Xu, X.; Li, S.; Shan, C.; Peng, W.; Chen, Y.; Li, S.; Peng, H.; Dai, T.; Zhou, E.; Bai, Y.; et al. Adhesively Bridging Co-Self-Assembled Monolayer and Perovskite Via In Situ Polymerization for Enhanced Stability of Inverted Perovskite Solar Cells. *Adv. Mater.* **2025**, *37*, 2505745. [CrossRef] [PubMed]

15. Brotchie, A. Medical devices: Soft micromachines run like clockwork. *Nat. Rev. Mater.* **2017**, *2*, 17002. [CrossRef]
16. Guo, Z.; Yuan, M.; Chen, G.; Liu, F.; Lu, R.; Yin, W. Understanding Defects in Perovskite Solar Cells Through Computation: Current Knowledge and Future Challenge. *Adv. Sci.* **2024**, *11*, 2305799. [CrossRef]
17. Chen, J.; Park, N.G. Materials and Methods for Interface Engineering toward Stable and Efficient Perovskite Solar Cells. *ACS Energy Lett.* **2020**, *5*, 2742–2786. [CrossRef]
18. Jiang, Q.; Zhao, Y.; Zhang, X.; Yang, X.; Chen, Y.; Chu, Z.; Ye, Q.; Li, X.; Yin, Z.; You, J. Surface passivation of perovskite film for efficient solar cells. *Nat. Photonics* **2019**, *13*, 460–466. [CrossRef]
19. Chen, C.; Zhao, X.; Gong, Y.; Liu, Y.; Chen, Z.; Zhang, L.; Chen, J.; Deng, Z.; Lu, H.; Luo, M.; et al. Two-Dimensional Hybrid Dion–Jacobson Germanium Halide Perovskites. *Chem. Mater.* **2023**, *35*, 3265–3275. [CrossRef]
20. Goetz, K.P.; Taylor, A.D.; Paulus, F.; Vaynzof, Y. Shining Light on the Photoluminescence Properties of Metal Halide Perovskites. *Adv. Funct. Mater.* **2020**, *30*, 1910004. [CrossRef]
21. Hacene, B.; Laufer, F.; Ternes, S.; Farag, A.; Pappenberger, R.; Fassl, P.; Moghadamzadeh, S.; Nejand, B.A.; Feeney, T.; Howard, I.; et al. Intensity Dependent Photoluminescence Imaging for In-Line Quality Control of Perovskite Thin Film Processing. *Adv. Mater. Technol.* **2024**, *9*, 2301279. [CrossRef]
22. Stoddard, R.J.; Eickemeyer, F.T.; Katahara, J.K.; Hillhouse, H.W. Correlation between Photoluminescence and Carrier Transport and a Simple In Situ Passivation Method for High-Bandgap Hybrid Perovskites. *J. Phys. Chem. Lett.* **2017**, *8*, 3289–3298. [CrossRef]
23. Wang, Z.; Ebadi, F.; Carlsen, B.; Choy, W.C.H.; Tress, W. Transient Photovoltage Measurements on Perovskite Solar Cells with Varied Defect Concentrations and Inhomogeneous Recombination Rates. *Small Methods* **2020**, *4*, 2000290. [CrossRef]
24. Guo, D.; Garmaroudi, Z.A.; Abdi-Jalebi, M.; Stranks, S.D.; Savenije, T.J. Reversible Removal of Intermixed Shallow States by Light Soaking in Multication Mixed Halide Perovskite Films. *ACS Energy Lett.* **2019**, *4*, 2360–2367. [CrossRef]

**Disclaimer/Publisher's Note:** The statements, opinions and data contained in all publications are solely those of the individual author(s) and contributor(s) and not of MDPI and/or the editor(s). MDPI and/or the editor(s) disclaim responsibility for any injury to people or property resulting from any ideas, methods, instructions or products referred to in the content.